

Article

Stability Improvement of Flexible Shallow Shells Using Neutron Radiation

Anton V. Krysko¹, Jan Awrejcewicz^{2,*} , Irina V. Papkova¹ and Vadim A. Krysko¹

¹ Department of Mathematics and Modeling Saratov State Technical University, 77 Politehnicheskaya Str., 410054 Saratov, Russia; anton.krysko@gmail.com (A.V.K.); ikravzova@mail.ru (I.V.P.); tak@san.ru (V.A.K.)

² Department of Automation, Biomechanics and Mechatronics, Lodz University of Technology, 1/15 Stefanowski St., 90-924 Lodz, Poland

* Correspondence: jan.awrejcewicz@p.lodz.pl

Received: 18 May 2020; Accepted: 14 July 2020; Published: 16 July 2020



Abstract: Microelectromechanical systems (MEMS) are increasingly playing a significant role in the aviation industry and space exploration. Moreover, there is a need to study the neutron radiation effect on the MEMS structural members and the MEMS devices reliability in general. Experiments with MEMS structural members showed changes in their operation after exposure to neutron radiation. In this study, the neutron irradiation effect on the flexible MEMS resonators' stability in the form of shallow rectangular shells is investigated. The theory of flexible rectangular shallow shells under the influence of both neutron irradiation and temperature field is developed. It consists of three components. First, the theory of flexible rectangular shallow shells under neutron radiation in temperature field was considered based on the Kirchhoff hypothesis and energetic Hamilton principle. Second, the theory of plasticity relaxation and cyclic loading were taken into account. Third, the Birger method of variable parameters was employed. The derived mathematical model was solved using both the finite difference method and the Bubnov–Galerkin method of higher approximations. It was established based on a few numeric examples that the irradiation direction of the MEMS structural members significantly affects the magnitude and shape of the plastic deformations' distribution, as well as the forces magnitude in the shell middle surface, although qualitatively with the same deflection the diagrams of the main investigated functions were similar.

Keywords: buckling; microstructures; stress relaxation; vibration

1. Introduction

Since thin-walled shells are highly efficient structural members, they have wide practical application. For example, they are used in instrument making, aerospace, petrochemical and nuclear industries. In general, shell structural elements can be made of various materials: concrete, reinforced concrete (supporting structures of nuclear reactors), various alloys and composites, etc. The mentioned materials can be used for fabrication of microelectromechanical systems (MEMS) including electromechanical relays, force and pressure sensors, accelerometers, digital logic switches, as well as biosensors and micromirrors. The latter composite devices are typically exposed to temperature and neutron irradiation as well as external force action during their working regimes. Hence, the use of novel and challenging MEMS designs and structural elements in space exploration to maintain the integrity of sensors and ensure operation in harsh conditions may play an important role for future space explorations.

In particular, flexible rectangular shallow shells are more useful for serving as MEMS resonators. The introduction of MEMS for operation in adverse environmental conditions, such as exposure to neutron irradiation and temperature risks, requires the use of new MEMS designs and structural

elements in order to maintain the integrity of sensors as well as to ensure operation under various conditions.

It should be emphasized that, if the requirement for strength and durability of materials is presented for structural elements in the macroscale, then for the microscale the change in the sensitivity and stable operation of the device under various input signal modes comes to the fore.

Already in 1953, Dienes [1] pointed out the importance of nuclear radiation with perspectives on changing the mechanical properties of solids. Not only did he show how the mechanical properties of crystalline substances—and in particular metals—can be produced by fast particle irradiation, but he also discussed how in high polymers nuclear radiation influenced the subsequent chemical reaction theory by altering their properties.

Further research on the analysis of stresses in metals caused by volumetric changes during neutron irradiation was carried out by Remnev [2,3]. Lensky [4] noted that a significant change in mechanical properties, considering the uneven volume distribution, requires clarification of existing and new theories as well as development of methods for calculating structural elements, especially if they are exposed to radiation fluxes during an operation. Ilyushin and Ogibalov [5] discussed the method of calculating the strength of thick-walled cylindrical shells in the presence of radiation. Norris [6] employed electron irradiation with the beam of a high voltage electron microscope to produce void growth in metals. Moreover, investigations of void growth effects were discussed for stainless steel and for nickel with emphasis on the moving dislocations and the surfaces. In the monograph by Likhachev and Pupko [7], the general theory relations of flow for irradiated materials were presented, based on the models proposed in the works of Birger for nonirradiated materials. Moreover, key generalizations for the governing equations of the plasticity and creep theory were made by taking into account irradiation with a neutron flux.

Singh et al. [8] studied the influence of irradiation with fission neutrons on specimens of pure copper and copper alloys. The change in volume due to irradiation as well as radiation damage of microstructures was reported.

Singh et al. [9] studied the features of neutron irradiation on microstructure and mechanical properties of pure iron by transmission electron microscopy. It was illustrated how interaction of cleared channels influenced the deformation and fracture behavior of the irradiated pure iron.

Garner et al. [10] studied swelling and creep phenomena irradiated in EBR-II. They illustrated how the swelling reached high levels rather quickly by reducing both fuel pin cladding interaction and the contribution of the irradiation to the total deformation.

Shea [11] reviewed the sensitivity of MEMS devices to radiation. The latter was linked primarily to the impact on device operation of radiation-induced trapped charge in dielectrics, with emphasis to electrostatic principles. It was illustrated how to increase radiation tolerance by design using either the actuation principle or electrical shielding of dielectrics.

Ghorbanpour Arani et al. [12] investigated the buckling of a cylindrical shell in the neutron radiation environment under combined static and periodic axial forces. They illustrated how the radiation induced porosity in elastic materials changed their thermal, electrical and mechanical properties. The carried out analysis was based on the classical shell theory. It was shown that both neutron induced swelling and temperature actions exhibited important effects on the stability and buckling of the cylindrical shell.

Sercombe et al. [13] used 3D simulation with an account of burnup-dependent pellet-clad friction while studied the power ramped cladding stresses during bare irradiation and ramp tests. They explained how the sole evolution of the friction coefficient with burnup captured the radial crack pattern of the rodlets after power ramping. Moreover, they derived a simple relation between the friction coefficient and the burnup variations.

Ben De Pauw [14] employed the optical fiber sensors to measure the fuel assembly vibration in a lead–bismuth eutectic cooled nuclear installation as input to assess vibration-related safety hazards.

Sitepu et al. [15] used palm fiber and palm shell as a thermal neutron radiation shielding material based on the neutron activation analysis and studied thermal neutron flux on gold pieces.

In studies [11–17], a generalized virtual modeling method using modern computer technologies to solve one-dimensional and two-dimensional nonlinear problems was proposed.

Srour et al. [18] carried out historical review of the literature regarding the radiation-induced displacement damage effects in semiconductor materials and devices. In particular, the effects of uniform radiation-induced displacement damage in bulk material and Si devices were outlined.

The increasing popularity of MEMS devices has led the researchers and engineers to study radiation-resistant resonators. Structural members of MEMS devices are micro-sized and very sensitive to external influences. They also depend on their respective operating principles. For example, for the oscillators used in GPS systems, one millionth of a percent is required for their operation stability, while the transistors used in integrated circuits can withstand parametric changes of several percent [18].

Babich [19] proposed mathematical models of radiation-induced physical processes in materials. Thermal and radiation strains dependent on the energy spectrum and components of radiation were estimated based on an appropriate analytical method. Moreover, the influence of the effects of radiations on the stress–strain state of thin plates was studied.

Marchal et al. [20] employed the finite element method to analyze the phenomenon of Pellet-Cladding interaction in nuclear fuel rods. The latter interaction produced high large stresses and led to failure. The fuel rods belong to the main members of nuclear water reactors and they consist of zirconium alloy tubes containing uranium dioxide pellets. The authors reported that the irradiation-induced phenomena yielded a densification of the fuel material in the irradiation early stages followed by solid swelling effects.

Semenov and Woo [21] modeled and analyzed dislocation structure development in metals and alloys with an account of anisotropic nucleation and dislocation loops subjected to actions of fast neutrons and external stresses. The stress-induced dislocation anisotropy was detected which exhibited a strong correlation with swelling. The nucleation kinematics was studied based on the derived Fokker-Planck equation.

Karahan and Buongiorno [22] formulated an engineering oriented code to predict the irradiation behavior of U–Zr and U–Pu–Zr metallic alloy and UO₂–PuO₂ mixed fuel pins in sodium-cooled fast reactors. Based on the introduced fuel pin geometry, composition and irradiation history, the authors studied numerically the fuel and clad thermomechanical behavior as both steady-state and design-basis transient scenarios.

Hall Jr. [23] derived the continuum plasticity model and studied the irradiation induced swelling of reactor core materials. It was shown that in the presence of significant swelling the deviatoric and volumetric strain rate components are functions of both deviatoric and hydrostatic components of stress for both linear and nonlinear creep.

Williamson [24] developed a powerful multidimensional fuels performance analysis having capability to simulate multi pellet steady and transient rod behavior based on the ABAQUS thermo mechanics code. Numerous input parameters were taken into account, including temperature, fuel densification, fission gas release during irradiation and gap heat transfer, etc.

The published experimental data presented in [18–24] show that, under the radioactive irradiation influence, a significant change is observed both in the thermo physical and elastic properties, as well as in the short-term and long-term mechanical characteristics of materials.

Karthik et al. [25] carried out the systematic microstructural studies of the austenitic stainless steel irradiation performance. The following salient features were analyzed: (a) behavior of SS316 at different fluence levels and (b) irradiation experiments of classical and modified D9 versions.

Fisher and Longo [26] carried out the creep analysis of slightly oval cylindrical shells under time-dependent loading, temperature and neutron flux. The influence of variations in neutron flux,

external pressure, mesh size and solution time step on collapse time was investigated based on the derived equilibrium equations.

NASA's Jet Propulsion Laboratory in Pasadena (JPL) developed micro and nano technologies for space exploration [27], while Sandia National Laboratory efforts to create radiation-strengthened inertial sensors [28]. The Defense Threat Reduction Agency (DTRA) of the United States has initiated several programs at several universities and government laboratories to study the radiation effects on a number of materials and structural elements of various MEMS and NEMS types. Investigations include silicon, silicon carbide, piezoelectric and ferroelectric, electro-optical and 2D materials, as well as studying the effect of radiation and thermal effects on the electrical, mechanical and optical properties and manifestations in various MEMS and NEMS operating modes.

In the last decade, exotic properties of pantographic metamaterials have been investigated and various mathematical models (both discrete and continuous) have been introduced.

It should be mentioned that the lack of studies devoted to stability of flexible rectangular shallow shells irradiated with neutrons may be partly due to the problem complexity, which is associated with the lack of an adequate mathematical model. At the same time, an experimental study of prototype structures both on a macro scale and on a micro scale is expensive and is associated with the destruction of test radioactive components. Therefore, there is a growing interest in using mathematical modeling methods to study various structural elements and our study aims at filling the existing gap in the so far described research.

The investigation of problem for the stability and stress-strain state of flexible shallow rectangular shells in terms of neutron irradiation is currently necessary both from a theoretical as well as practical point of view. This observation follows from a critical review of the works [29–31].

This work is devoted to the modeling and prediction problem of the flexible rectangular shallow shell stability subjected to neutron irradiation, used as MEMS resonators. The validity of our research can be also justified based on the observation that to the best of our knowledge, a study of the geometrically and physically nonlinear shells stability under the neutron irradiation action has not been done.

The study is organized in the following way. The shell mathematical model is introduced in Section 2, whereas the employed computational methods are presented in Section 3. The reliability and validity of the obtained results are discussed in Section 4. Section 5 deals with the account of the residual shell plastic deformations and the numeric examples are reported in Section 6. Section 7 presents the concluding remarks.

2. Problem Statement

We consider a shell of length a , with thickness $2h$ and width b . It occupies the volume $\Omega = \{0 \leq x \leq a; 0 \leq y \leq b; -h \leq z \leq h\}$, where x, y, z are spatial coordinates (Figure 1).

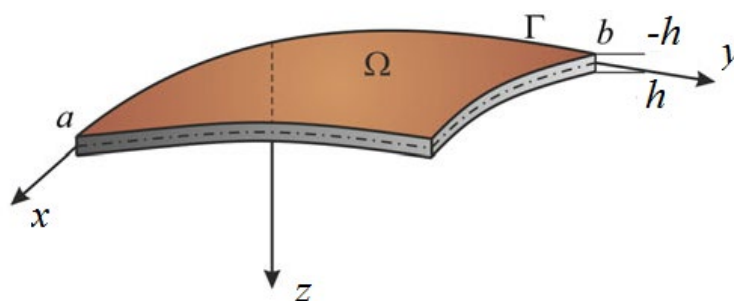


Figure 1. Computational shell scheme.

The following hypotheses hold:

- (i) the Kirchhoff–Love kinematic shell model is taken where strain tensor components for the middle shell surface are $\varepsilon_{xx} = -z \frac{\partial^2 w}{\partial x^2}$, $\varepsilon_{yy} = -z \frac{\partial^2 w}{\partial y^2}$ and $w(x, y, t)$ denotes shell deflection at its middle surface;
- (ii) the shell material is isotropic, but nonhomogenous and its properties depend on temperature, $T(x, y, z)$, i.e., we have elastic modulus E and Poisson's ratio ν are constants at the initial time moment and then the functions $E = E(x, y, z, e_r, T(x, y, z), \alpha(T))$, $\nu = \nu(x, y, z, e_r, T(x, y, z), \alpha(T))$ and the shell deformed state depends on temperature at a point (x, y, z) ;
- (iii) Duhamel–Neumann law is adopted, i.e., we have $\varepsilon_{xx}^z = \varepsilon_{xx} + \varepsilon_{xx}^{1p} + \alpha T(x, y, z)$, $\varepsilon_{yy}^z = \varepsilon_{yy} + \varepsilon_{yy}^{1p} + \alpha T(x, y, z)$, $\varepsilon_{xy}^z = \varepsilon_{xy} + \varepsilon_{xy}^{1p}$, where α stands for coefficient of linear thermal extension and ε_{xx}^{1p} , ε_{yy}^{1p} , ε_{xy}^{1p} are plastic components of the strain tensor components at the unloading time;
- (iv) theory of plasticity and Mises criterion are used;
- (v) deformation diagrams $\sigma_r(e_r, T, \alpha)$ depend both on shell temperature and its stress–strain state, where σ_r stands for intensity of tensions and e_r is deformation intensity;
- (vi) the temperature field is defined by a 3D heat-transfer equation without any restrictions put on temperature distribution.

The mathematical model is yielded by the Hamilton's variational principle. The shell accumulated potential energy is:

$$\Pi = \frac{1}{2} \int_{-h}^h dz \int_0^a \int_0^b (\sigma_{xx} \varepsilon_{xx} + \sigma_{yy} \varepsilon_{yy} + 2\sigma_{xy} \varepsilon_{xy}) dx dy, \quad (1)$$

where σ_{xx} , σ_{yy} , σ_{xy} —stress tensor components for the shell middle surface.

Moreover, the works of external forces.

$$\delta' W = \int_0^a \int_0^b q \delta w dx dy. \quad (2)$$

where q —external transverse uniformly distributed load.

Stress–strain state of nonhomogenous plates and shallow rectangular shells is governed by the following nonlinear PDEs:

$$\begin{pmatrix} L_{11} & L_{12} \\ L_{21} & L_{22} \end{pmatrix} \cdot \begin{pmatrix} w \\ F \end{pmatrix} + \begin{pmatrix} L & 0 \\ 0 & -\frac{1}{2}L \end{pmatrix} \cdot \begin{pmatrix} w, F \\ w, w \end{pmatrix} = - \begin{pmatrix} Q_1 \\ Q_2 \end{pmatrix}, \quad (3)$$

where F is the load function and the linear operators with variable coefficients are defined in the following way:

$$\begin{aligned}
 L_{11}(\bullet) &= \frac{\partial^2}{\partial x^2} \left(\lambda^{-1} B_{11}^0 \frac{\partial^2(\cdot)}{\partial x^2} + B_{10}^* \frac{\partial^2(\cdot)}{\partial y^2} \right) + \\
 &+ 2 \frac{\partial^2}{\partial x \partial y} \left[(B_{11}^* - B_{10}^*) \frac{\partial^2(\cdot)}{\partial x \partial y} \right] + \frac{\partial^2}{\partial y^2} \left(B_{10}^* \frac{\partial^2(\cdot)}{\partial x^2} + \lambda^2 B_{11} \frac{\partial^2(\cdot)}{\partial y^2} \right), \\
 L_{12}(\bullet) &= \nabla_k^2(\cdot) + \frac{\partial^2}{\partial x^2} \left(B_{10} \frac{\partial^2(\cdot)}{\partial y^2} + \lambda^2 B_{11} \frac{\partial^2(\cdot)}{\partial x^2} \right) - \\
 &- 2 \frac{\partial^2}{\partial x \partial y} \left[(B_{10} - B_{11}) \frac{\partial^2(\cdot)}{\partial x \partial y} \right] + \frac{\partial^2}{\partial y^2} \left(B_{11} \lambda^2 \frac{\partial^2(\cdot)}{\partial y^2} + B_{10} \frac{\partial^2(\cdot)}{\partial x^2} \right), \\
 L_{21}(\bullet) &= \nabla_k^2(\cdot) + \frac{\partial^2}{\partial x^2} \left(B_{11} \lambda^{-2} \frac{\partial^2(\cdot)}{\partial x^2} + B_{10} \frac{\partial^2(\cdot)}{\partial y^2} \right) - \\
 &- 2 \frac{\partial^2}{\partial x \partial y} \left[(B_{10} - B_{11}) \frac{\partial^2(\cdot)}{\partial x \partial y} \right] + \frac{\partial^2}{\partial y^2} \left(B_{10} \lambda^{-2} \frac{\partial^2(\cdot)}{\partial x^2} + B_{11} \frac{\partial^2(\cdot)}{\partial y^2} \right), \\
 L_{22}(\bullet) &= \frac{\partial^2}{\partial x^2} \left(A_2 \frac{\partial^2(\cdot)}{\partial y^2} - \lambda^{-2} A_1 \frac{\partial^2(\cdot)}{\partial x^2} \right) + \\
 &+ \frac{\partial^2}{\partial y^2} \left(\lambda^2 A_1 \frac{\partial^2(\cdot)}{\partial y^2} + A_2 \frac{\partial^2(\cdot)}{\partial x^2} \right) + 2 \frac{\partial^2}{\partial x \partial y} \left[(A_1 - A_2) \frac{\partial^2(\cdot)}{\partial x \partial y} \right].
 \end{aligned}
 \tag{4}$$

and:

$$L((\bullet), (\bullet)) = \frac{\partial^2(\cdot)}{\partial x^2} \frac{\partial^2(\cdot)}{\partial y^2} - 2 \frac{\partial^2(\cdot)}{\partial x \partial y} \frac{\partial^2(\cdot)}{\partial x \partial y} + \frac{\partial^2(\cdot)}{\partial y^2} \frac{\partial^2(\cdot)}{\partial x^2}
 \tag{5}$$

where λ stands for the length to width ratio.

The right hand sides of the governing equations with an account of transversal load and residual elastic–plastic deformations (with account of loading history) have the following form:

$$\begin{aligned}
 Q_1 &= \lambda^{-1} \frac{\partial^2}{\partial x^2} (B_{10} T_{xx}^0 + B_{11} T_{yy}^0) + 2 \frac{\partial^2}{\partial x \partial y} [(B_{10} - B_{11}) T_{xy}^0] + \lambda \frac{\partial^2}{\partial y^2} (B_{11} T_{xx}^0 + B_{10} T_{yy}^0) - \\
 &- \lambda^{-1} \frac{\partial^2 T_{xx}^1}{\partial x^2} - 2 \frac{\partial^2 T_{xy}^1}{\partial x \partial x} - \lambda \frac{\partial^2 T_{yy}^1}{\partial y^2} + q, \\
 Q_2 &= \lambda^{-2} \frac{\partial^2}{\partial x^2} (A_2 T_{xx}^0 + A_1 T_{yy}^0) + \lambda \frac{\partial^2}{\partial y^2} (A_1 T_{xx}^0 + A_2 T_{yy}^0) - 2 \frac{\partial^2}{\partial x \partial y} [(A_1 - A_2) T_{xy}^0],
 \end{aligned}
 \tag{6}$$

stands for nonlinear operators, where, $T_{xx}^0, T_{yy}^0, T_{xx}^1, T_{xy}^1, T_{yy}^1$ —contain temperature components and residual plastic deformations.

The relations between dimensional and nondimensional (bars) parameters are as follows:

$$\begin{aligned}
 E &= G_0 \bar{E}, \quad G = G_0 \bar{G}, \quad K = G_0 \bar{K}, \quad q = G_0 \frac{(2h_0)^4}{a^2 b^2} \bar{q}, \quad T_{xx}^0 = G_0 \frac{(2h_0)^3}{ab} \bar{T}_{xx}^0, \quad F = G_0 (2h_0)^3 \bar{F}, \\
 T_{yy}^0 &= G_0 \frac{(2h_0)^3}{ab} \bar{T}_{yy}^0, \quad F = G_0 (2h_0)^3 \bar{F}, \quad T_{xx}^1 = G_0 \frac{(2h_0)^3}{ab} \bar{T}_{xx}^1, \\
 T_{yy}^1 &= G_0 \frac{(2h_0)^3}{ab} \bar{T}_{yy}^1, \quad K_x = (2h_0) a^{-2} \bar{K}_x, \quad K_y = (2h_0) b^{-2} \bar{K}_y, \quad B_{ik} = G_0 (2h_0)^3 \bar{B}_{ik}, \\
 E_{ij} &= G_0 (2h_0)^{i+1} \bar{E}_{ij}, \quad (i = 0, \dots, 4, \quad j = 0, 1), \quad e_r = \left(\frac{2h_0}{a} \right)^2 \bar{e}_r, \quad e_s = \left(\frac{2h_0}{a} \right)^2 \bar{e}_s, \quad h = \bar{h} h_0, \\
 A_j &= \frac{1}{G_0 (2h_0)} \bar{A}_j, \quad (k = 1, 2), \quad \lambda = \frac{a}{b}, \quad w = (2h_0) \bar{w}, \quad x = a \bar{x}, \quad y = b \bar{y}.
 \end{aligned}
 \tag{7}$$

where: G_0 —the shear modulus characteristic value in the undeformed state; G —shear modulus; K —volumetric compression ratio; h_0 —shell thickness in its center; K_x, K_y —shell curvatures in x and y directions, respectively and e_s —fluidity deformation.

Integrals with regard to shell thickness follow:

$$\begin{aligned}
 E_{ij} &= \int_{-h}^h \frac{Ez^i}{1+(-1)^j \nu} dz, \\
 T_{xx}^j &= \int_{-h}^h \frac{Ez^j}{1-\nu^2} (\varepsilon_{xx}^T + \nu \varepsilon_{yy}^T) dz, \quad T_{yy}^j = \int_{-h}^h \frac{Ez^j}{1-\nu^2} (\varepsilon_{yy}^T + \nu \varepsilon_{xx}^T) dz, \\
 T_{xy}^j &= \int_{-h}^h \frac{Ez^j}{2(1+\nu)} \varepsilon_{xy}^T dz \quad (i = 0, \dots, 4, \quad j = 0, 1),
 \end{aligned}
 \tag{8}$$

where $\varepsilon_{xx}^T = \alpha T + e_{xx}^{1p}$, $\varepsilon_{yy}^T = \alpha T + e_{yy}^{1p}$, $\varepsilon_{xy}^T = e_{xy}^{1p}$ stand for deformation depending on temperature and plastic deformation components of the deformation tensor in either relaxation ‘1P’ or at the time instant of the secondary loading (“2P”); as it was already mentioned that α is the coefficient of linear thermal expansion and T stands for the temperature function, whereas:

$$\begin{aligned}
 A_j &= \frac{1}{2} \left(\frac{1}{E_{01}} + (-1)^{j+1} \frac{1}{E_{00}} \right), \\
 B_{ik} &= \frac{1}{2ih^{i-1}} \left(\frac{E_{i0}}{E_{01}} + (-1)^k \frac{E_{i0}}{E_{00}} \right), \quad (i = 1, 3; \quad j = 1, 2; \quad k = 0, 1).
 \end{aligned}
 \tag{9}$$

The matrix $\begin{pmatrix} L_{11} & L_{12} \\ L_{21} & L_{22} \end{pmatrix}$ is symmetric, as in the case of an elastic problem (this observation is yielded by Betti’s theorem).

The governing Equations (3) are nondimensional (bars are omitted). It should be mentioned that PDEs (3) are obtained based on the kinematic Kirchhoff–Love model and the method of variable elasticity parameters [32]. The derivation of the governing equations is based on the theory of plasticity where E and ν are coupled with the shear modulus G and the bulk modulus K via the following relations:

$$E = \frac{9KG}{3K + G}, \quad \nu = \frac{1}{2} \frac{3K - 2G}{3K + G}
 \tag{10}$$

The following simplifications are introduced. We take $K = K_0 = const$ and owing to the hypothesized small elastic–plastic deformations, we have:

$$G = \frac{1}{3} \frac{\sigma_r(e_r)}{e_r},
 \tag{11}$$

where σ_r stands for the stress intensity, e_r , describes the deformation intensity:

$$e_r = \frac{\sqrt{2}}{3} \left[(e_{xx} - e_{yy})^2 + (e_{yy} - e_{zz})^2 + (e_{xx} - e_{zz})^2 + 1.5e_{xy}^2 \right]^{1/2},
 \tag{12}$$

and the following plane stress state formula holds:

$$e_{zz} = -\frac{\nu}{1-\nu} (e_{xx} + e_{yy}),
 \tag{13}$$

where e_{xx} , e_{yy} , e_{zz} , e_{xy} are the strain tensor components for an arbitrary shell point.

It should be emphasized that ν is not constant.

3. Computational Method

In order to carry out the numeric computations, the dependence $\sigma_r(e_r)$ can be defined in an arbitrary way. The system of nonlinear PDEs (3) is solved by the variational Bubnov–Galerkin method

in higher approximations in the form proposed by Vlasov [33]. Namely, the system of approximating functions is assumed in the following form

$$w = \sum_{c,b=1}^N P_{c,b} w_{c,b}(x, y), \quad F = \sum_{c,b=1}^N R_{c,b} F_{c,b}(x, y). \tag{14}$$

where $w_{c,b}$ and $F_{c,b}$ stands for the system of approximating functions; c, b are the series terms number; $P_{c,b}, R_{c,b}$ are constants to be determined from the Bubnov–Galerkin procedure.

In order to find the approximate value of the element w and F , we choose the coordinate systems of functions $\{w_{c,b}(x,y), F_{c,b}(x,y)\}$ ($c, b = 0, 1, 2, \dots$) in (14), satisfying the following five requirements:

1. $w_{c,b}(x,y) \in H_A, F_{c,b}(x,y) \in H_A$, where H_A is the Hilbert space, which we will call the energy space.
2. $\forall c, b$ functions $w_{c,b}(x,y)$ and $F_{c,b}(x,y)$ are linearly independent, continuous together with their partial derivatives up to the fourth order inclusive in the region Ω .
3. $w_{c,b}(x,y)$ and $F_{c,b}(x,y)$ satisfy the main boundary conditions (and the initial conditions, if any) exactly.
4. $w_{c,b}(x,y)$ and $F_{c,b}(x,y)$ have the completeness property in H_A .
5. $w_{c,b}(x,y)$ and $F_{c,b}(x,y)$ must represent the N first elements of a function’s complete system.

We substitute (14) into (3) and after employment of the Bubnov–Galerkin procedure, the following system of nonlinear algebraic equations is obtained

$$\begin{pmatrix} a_{11} & a_{12} \\ a_{21} & a_{22} \end{pmatrix} \cdot \begin{pmatrix} P \\ R \end{pmatrix} + \begin{pmatrix} a_{13} & 0 \\ 0 & -a_{23} \end{pmatrix} \cdot \begin{pmatrix} M \\ N \end{pmatrix} + \begin{pmatrix} \bar{Q}_1 \\ \bar{Q}_2 \end{pmatrix} = 0, \tag{15}$$

where:

$$P = \begin{pmatrix} P_{11} \\ P_{12} \\ \vdots \\ P_{1N} \\ \vdots \\ P_{NN} \end{pmatrix}, \quad R = \begin{pmatrix} R_{11} \\ R_{12} \\ \vdots \\ R_{1N} \\ \vdots \\ R_{NN} \end{pmatrix}, \quad M = \begin{pmatrix} M_{1111} \\ M_{1112} \\ \vdots \\ M_{111N} \\ \vdots \\ M_{NNNN} \end{pmatrix}, \quad N = \begin{pmatrix} N_{1111} \\ N_{1112} \\ \vdots \\ N_{111N} \\ \vdots \\ N_{NNNN} \end{pmatrix}. \tag{16}$$

We substitute $\left(\sum_{c,b=1}^N P_{c,b}\right) \times \left(\sum_{k,l=1}^N R_{k,l}\right)$ and $\left(\sum_{c,b=1}^N P_{c,b}\right) \times \left(\sum_{k,l=1}^N P_{k,l}\right)$ by $M_{c,b,k,l}$ and $N_{c,b,k,l}$ respectively, where:

$$\begin{aligned} a_{11} &= \left(\int_0^1 \int_0^1 (L_{11}(w_{c,b})) w_{f,v} dx dy \right)_{f,v=1}^{f,v=N}, & a_{12} &= \left(\int_0^1 \int_0^1 (L_{12}(F_{c,b})) w_{f,v} dx dy \right)_{f,v=1}^{f,v=N}, \\ a_{21} &= \left(\int_0^1 \int_0^1 (L_{21}(F_{c,b})) w_{f,v} dx dy \right)_{f,v=1}^{f,v=N}, & a_{22} &= \left(\int_0^1 \int_0^1 (L_{22}(F_{c,b})) w_{f,v} dx dy \right)_{f,v=1}^{f,v=N}, \\ a_{13} &= \left(\int_0^1 \int_0^1 (L(w_{c,b}, F_{c,b})) w_{f,v} dx dy \right)_{f,v=1}^{f,v=N}, & a_{23} &= \left(\frac{1}{2} \int_0^1 \int_0^1 (L(w_{c,b}, w_{c,b})) F_{f,v} dx dy \right)_{f,v=1}^{f,v=N}, \\ \bar{Q}_1 &= \left(\int_0^1 \int_0^1 Q_1 w_{f,v} dx dy \right)_{f,v=1}^{f,v=N}, & \bar{Q}_2 &= \left(\int_0^1 \int_0^1 Q_2 F_{f,v} dx dy \right)_{f,v=1}^{f,v=N}. \end{aligned} \tag{17}$$

In order to solve the elastic–plastic problems through the Bubnov–Galerkin method (BGM), the program written in C++ is realized in the following way.

The following quantities are first introduced: geometric (λ , K_x , K_y) and physical (K , E , ν , e_s) parameters, the analytical dependence σ_r (e_r) computational steps with regard to load Δq or shell center deflection Δw . Then the form of the approximating functions is defined depending on the introduced boundary conditions. In addition, we introduce the load type $q(x, y)$.

While employing the method of variable elasticity parameters, the computational process is realized in the following way. Having in hand the initial values of E , ν , K , formulas (8) and (9) yield the values of E_{ij} , A_j , B_{ik} defined at the shell point (x_n, y_m) . Then the system of Equation (15) is constructed. The Newton's method yields the coefficients P_{ij} and R_{ij} with regard to Equation (14). The formulas:

$$\begin{aligned} e_{xx} &= \varepsilon_{11} + z\chi_{11}, & e_{yy} &= \varepsilon_{22} + z\chi_{22}, & e_{xy} &= \varepsilon_{12} + z\chi_{12}, \\ \varepsilon_{11} &= A_1T_1 + A_2T_2 - B_{10}\chi_{11} - B_{11}\chi_{22} + A_1T_{xx}^0 + A_2T_{yy}^0, \\ \varepsilon_{22} &= A_2T_1 + A_1T_2 - B_{10}\chi_{22} - B_{11}\chi_{11} + A_2T_{xx}^0 + A_1T_{yy}^0, \\ \varepsilon_{12} &= 2(A_1 - A_2)S + (B_{10} - B_{11})\chi_{12}, \\ \chi_{11} &= -\frac{\partial^2 w}{\partial x^2}, & \chi_{22} &= -\frac{\partial^2 w}{\partial y^2}, & \chi_{12} &= -2\frac{\partial^2 w}{\partial x \partial y} \end{aligned} \quad (18)$$

allow to estimate deformations of the shell volume as well as the deformations intensity (relation (12)), and then Equations (10) and (11) yielded the shear modulus. In addition, the E and ν are numerically estimated at each point of the shell volume. However, as to be expected, the obtained values differ from the initial state. In order to avoid the problems of divergence, a new value of ν was substituted to Equation (12). Next, the improved value of e_r is obtained, and new values of E and ν are defined. The mentioned internal process of iterations is repeated until the required accuracy is achieved and the obtained values of $E(x_n, y_m, z_p)$, $\nu(x_n, y_m, z_p)$ are stored in the computer's memory, where x_n , y_m , z_p are the coordinates of the points set into which the shell volume is divided. Repeating the so far described computations for all z_p the integration is carried out with regard to z and finally, the values of E_{ij} , A_j , B_{ik} as functions of x, y are defined.

However, the obtained values (usually) differ from the initial ones. They are taken again to carry out the computational process unless the given computational accuracy is achieved.

In order to solve the elastic-plastic problems of a considered shell we take the values of E_{ij} , A_j , B_{ik} for linear elastic material as the first approximation. Then, the successive approximation of E_{ij} , A_j , B_{ik} is achieved based on the values from the previous shell loading step. The latter choice of initial approximations allows for determination of E and ν by two to three iterations keeping the assumed accuracy of $\varepsilon = 10^{-5}$.

4. Reliability of the Obtained Results

A solution of the system of nonlinear algebraic Equations (15) which are obtained by the Bubnov-Galerkin procedure are found with the help of the Newton's iterative method. Integrations are carried out using the Newton-Cotes quadrature rules, where the shell volume is partitioned into $13 \times 13 \times 6$ parts with regard to x, y, z , respectively.

Numeric differentiations are carried out with the help of finite-difference formulas. Owing to the worked out case studies, the shell volume partitions of $26 \times 26 \times 12$ satisfy the required accuracy, and hence the obtained solution is reliable. In the case when the shell is supported by flexible non-stretched (nonelongated) ribs on its contour, and is subjected to uniformly distributed constant load, the following boundary conditions hold

$$w = T_{xx}^1 = T_{yy}^0 = \varepsilon_{yy} = 0, \quad w = T_{yy}^1 = T_{xx}^0 = \varepsilon_{xx} = 0, \quad (19)$$

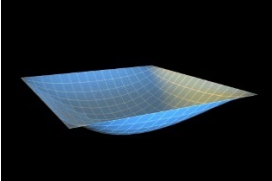
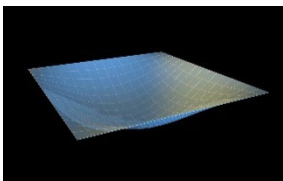
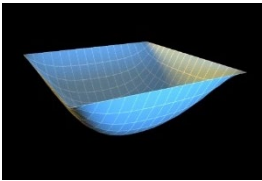
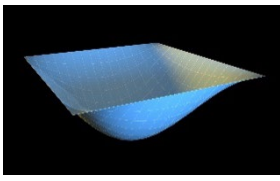
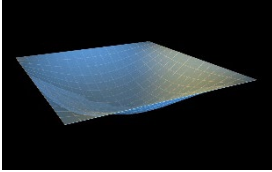
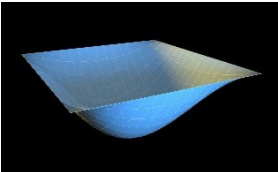
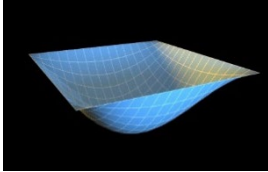
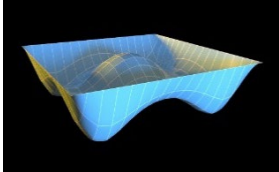
where T_{xx}^1, T_{yy}^1 stand for the moments and T_{xx}^0, T_{yy}^0 for the forces defined at the shell center with regard to x and y .

The system of approximating functions satisfying the boundary conditions (19) take the following form

$$w_{c,b} = F_{c,b} = \sin(c\pi x) \sin(b\pi y). \tag{20}$$

In order to check reliability of the used approach, we have compared the results obtained by the Bubnov–Galerkin method in higher approximations ($N = 5$) and by the finite differences method (FDM) of second order accuracy ($n \times n = 32 \times 32$). Figure 2a shows the load–deflection graph depending on the grid nodes number in the finite differences method of the second accuracy order for an elastic plate (8×8 ; 13×13 ; 26×26 ; 32×32). These results show that a 13×13 grid partition is sufficient to solve static problems. For an elastoplastic problem, a spatial grid of $13 \times 13 \times 6$ is sufficient. Further studies were carried out with a partition of $13 \times 13 \times 6$. We have fixed the shell curvatures $K_x = K_y = 0$, $K_x = K_y = 24$, and then the set up method was employed (see [34,35]). Table 1 presents the surfaces of deflection and stresses for the plate ($K_x = K_y = 0$) and the shell ($K_x = K_y = 24$) for the cases of pre-critical ($q = 120$) and postcritical ($q = 300$) loads. In the case of plate, the stress/deflection distribution character does not change qualitatively with regard to the load increase. In the case of the shell, the stress (Airy’s) function is positive (negative) for the pre-critical (postcritical) state, i.e., it changes its sign that serves as its stability criterion.

Table 1. Surfaces of deflection and stress of the plate and the shell.

$K_x = K_y = 0$ (plate)			
$q = 150$ (Point A (2, 150))		$q = 280$ (Point B (2.8, 280))	
Deflection $w(x, y)$	Moment $\frac{M_x + M_y}{2}$	Deflection $w(x, y)$	Moment $\frac{M_x + M_y}{2}$
			
$K_x = K_y = 24$ (shell)			
$q = 150$ (Point C (0.5, 150))		$q = 280$ (Point D (8.4, 280))	
Deflection $w(x, y)$	Average moment $\frac{M_x + M_y}{2}$	Deflection $w(x, y)$	Moment $\frac{M_x + M_y}{2}$
			

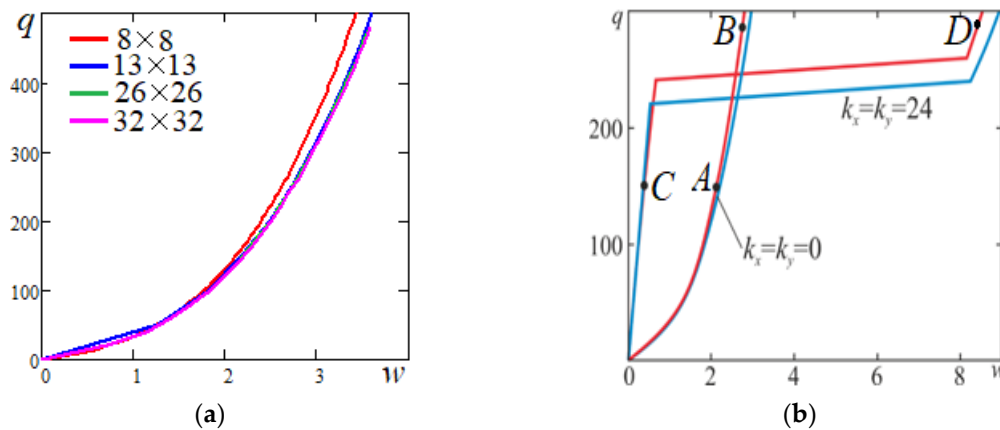


Figure 2. Dependence “load–deflection” (a) graphs comparison with different nodes number in the grid; (b) in the shell center obtained via the Bubnov–Galerkin method (BGM) in higher accuracy approximation (blue) and finite differences method (FDM) (red).

5. Algorithms for Account of the Residual Plastic Deformations

We take the dependence $\sigma_r(e_r)$ shown in Figure 3 and we trace a loading relaxation history of the shell element

$$\begin{aligned} \sigma_r &= 3G_0 e_r \text{ for } e_r < e_s, \\ \sigma_r &= 3G_0 e_r + 3G_1(e_r - e_s) \text{ for } e_r \geq e_s, \end{aligned} \tag{21}$$

and:

$$\begin{aligned} G &= G_0 \text{ for } e_r < e_s, \\ G &= \frac{G_0 e_s}{e_r} + G_1 \left(1 - \frac{e_s}{e_r}\right) \text{ for } e_r \geq e_s, \end{aligned} \tag{22}$$

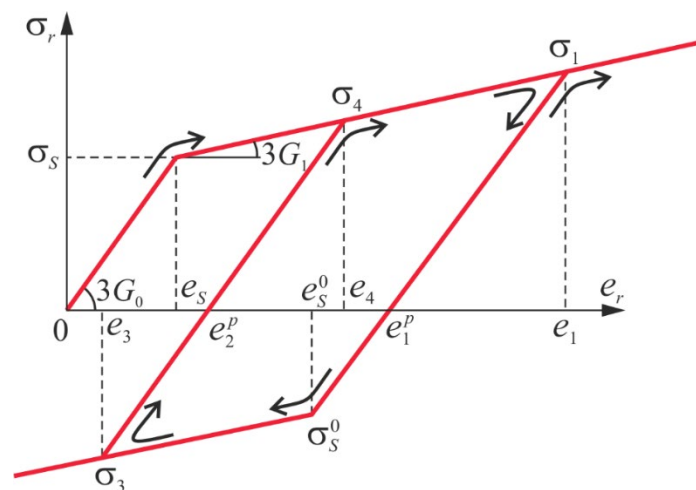


Figure 3. Dependence $\sigma_r(e_r)$ constructed based on formulas (21) and (22).

In Figure 3 area $(0; 0); (e_s; \sigma_s)$ describes elastic shell deformation, $(e_s; \sigma_s); (e_1; \sigma_1)$ stand for the shell plastic deformation, unloading in the plastic deformation zone occurs in a straight line $(e_1; \sigma_1); (e_s^0; \sigma_s^0)$ and secondary plastic deformations are denoted by $(e_s^0; \sigma_s^0); (e_3; \sigma_3), (e_3; \sigma_3); (e_4; \sigma_4)$. The shell deformation process can be followed beginning from its counterpart nondeformed state and hence various variants of composition a computations of the quantities $e_{xx}^{1p}, e_{yy}^{1p}, e_{xy}^{1p}, G$ can be numerically realized. We present and illustrate this possibility for an arbitrary chosen shell element.

Assume the considered shell element be under the active loading process where $de_r > 0$. The shear modulus G , owing to the Mises criterion of plasticity, is equal to G_0 and the quantities e_{xx}^{1p} , e_{yy}^{1p} , e_{xy}^{1p} are equal to zero. If $e_r \geq e_s$, the shear modulus is defined by the formula:

$$G = G_0 \frac{e_s}{e_r} + G_1 \left(\frac{e_r - e_s}{e_r} \right). \tag{23}$$

The quantities e_{xx}^{1p} , e_{yy}^{1p} , e_{xy}^{1p} , e_1^p get the following new values (on each stage of the loading process until $de_r > 0$)

$$\begin{aligned} e_{xx}^{1p} &= e'_{xx} - \frac{1}{E} (\sigma'_{xx} - \nu \sigma'_{yy}), \\ e_{yy}^{1p} &= e'_{yy} - \frac{1}{E} (\sigma'_{yy} - \nu \sigma'_{xx}), \\ e_{xy}^{1p} &= e'_{xy} - \frac{2(1+\nu)}{E} \sigma'_{xy}, \\ \sigma_r &= 3G_0(e_r - e_1^p). \end{aligned} \tag{24}$$

The quantities with primes are defined in the beginning of the loading, whereas E and ν are computed using formulas (10) and they do not influence further computations (18). We need to recompute the quantities e_{xx}^{1p} , e_{yy}^{1p} , e_{xy}^{1p} , e_1^p at each stage of the active loading process, since the loading process may change its sign on at arbitrary loading stage. The latter requires knowledge of the last deformations e_{xx}^{1p} , e_{yy}^{1p} , e_{xy}^{1p} , and their intensity e_1^p on the previous loading stage, which in this case is known as the beginning of relaxation (it should be mentioned that an account of the loading and relaxation history is realized with accuracy up to the loading step).

In this relaxation case under the condition of lack of the plastic deformation, we have:

$$de_r \leq 0, \quad e_r < e_1, \quad G = G_0 \frac{e_r - e_1^p}{e_r} \tag{25}$$

and the quantities e_{xx}^{1p} , e_{yy}^{1p} , e_{xy}^{1p} are introduced into (18). If, after that the loading process is activated then unless $e_k < e_1$, the G modulus is defined by (25) and e_{xx}^{1p} , e_{yy}^{1p} , e_{xy}^{1p} take part in the computations. However, if $e_r > e_1$, the modulus G is defined through (23) and the quantities e_{xx}^{1p} , e_{yy}^{1p} , e_{xy}^{1p} and e_1^p are compared to zero, i.e., they do not appear in (18) but they get new values.

In the case of relaxation associated with the secondary plastic deformations, which corresponds to the fourth part of dependence $\sigma_r(e_r)$ (see Figure 3), we have:

$$\sigma_r = -3G_0 + 3G_1(e_r + e_s). \tag{26}$$

Here, we consider the material which obeys ideal Bauschinger’s effect with:

$$G = -G_0 \frac{e_s}{e_r} + G_1 \frac{e_r + e_s}{e_r}, \quad de_r < 0, \quad e_r < e_s^0. \tag{27}$$

Here the quantities e_{xx}^{1p} , e_{yy}^{1p} , e_{xy}^{1p} and e_1^p obtained in the time instant of the relaxation beginning are taken into account in the further computations process. If, after that, we have $de_r > 0$ (fifth part of the dependence $\sigma_r(e_r)$), then

$$G = G_0 \frac{e_r - e_2^p}{e_r}, \tag{28}$$

and instead of the quantities e_{xx}^{1p} , e_{yy}^{1p} , e_{xy}^{1p} , e_1^p , the quantities e_{xx}^{2p} , e_{yy}^{2p} , e_{xy}^{2p} , e_2^p are introduced. The latter are obtained on the last relaxation stage of the interval $e_3 < e_r < e_s^0$ with regard to formulas (24) (here instead of values with one touch we use values with two touches found in a repeated load moment). However, the relaxation process can again change its sign ($de_r < 0$) and if $e_r > e_3$ the modulus G is defined by formula (28) with inclusion of the quantities e_{xx}^{2p} , e_{yy}^{2p} , e_{xy}^{2p} , e_2^p .

If $e_r < e_3$, then G is defined by (27) and we take $e_{xx}^{2p}, e_{yy}^{2p}, e_{xy}^{2p}, e_2^p$ instead of $e_{xx}^{2p}, e_{yy}^{2p}, e_{xy}^{2p}, e_1^p$. Finally, if the secondary loading stage (fifth part) for $de_r > 0$ is accompanied by the change of the plastic deformations, then for $e_r > e_4$ shear modulus G is governed by formula (23), whereas the quantities $e_{xx}^{1p}, e_{yy}^{1p}, e_{xy}^{1p}, e_1^p$ are taken as equal to zero. Then, at each computational stage the quantities $e_{xx}^{3p}, e_{yy}^{3p}, e_{xy}^{3p}, e_3^p$ are computed based on formulas (24), which opens the new cycle origin of the “load-relaxation” process.

In what follows we consider the neutron radiations of flexible rectangular shells stability. Lenskiy [4] pointed out that metal radiation through the fast neutrons flux implies change of their physical and metallic properties. It was observed that the largest radiation influence was exhibited by the magnitude of the carbon silicate material flow limit σ_s . Radiation increase implies increase of σ_s . In the steel F-212 V case, the functional and nonlinear dependence of σ_s versus the total radiation flux is reported by Iliushin and Ogibalov [5].

If the radiation flux is perpendicular to material surface, then the dependence of the total versus amplitude can be approximated through the following formula [36]:

$$N = N_0 e^{2h(1 \pm z)}, \quad -1 \leq z \leq 1. \quad (29)$$

Assuming the following fixed parameters: $2h = 2$, $N_0 = 4 \times 10^{19} nvt$, $\left(\frac{a}{2h_0}\right)^2 = 1000$, $G_0 = 0.8 \times 10^6$ bar, $\nu = 0.3$, $G_1 = 0$ the plasticity flow limit is governed by the following formula:

$$\sigma_s(z) = (5000 \pm 1800z) \quad (30)$$

whereas the reported deformation intensity at the instant of the plasticity beginning is governed by the following formula:

$$e_s = 2.08 \pm 0.75z. \quad (31)$$

Here the signs minus (–) and plus (+) refer to the shell radiation direction from its convexity and concavity, respectively. In the case of nonradiated material, we have $\sigma_s = 3375$ bar, a $e_s = 1.405$.

Observe that in the latter case of the study, the radiation influence by the fast neutrons flux, the computational problem is reduced to computation of the plastic nonhomogenous (with regard to thickness) flexible shell made from an ideal elastic–plastic material. It should be mentioned that the worked out algorithm accepts arbitrary form of the dependence $\sigma_s(z)$, i.e., its either analytical or digital form.

6. Numeric Experiments and the Results Discussion.

In what follows we consider examples of the radiation direction influence on the shell behavior. The following geometric shell parameters are fixed: $K_x = K_y = 16$, $K_x = K_y = 24$.

The system of approximating functions to the computational solution is taken in the form of (20) and it satisfies the boundary conditions (19).

The computations are carried out in the way described earlier. We have taken $N = 3$ in (14), since further increase of the series terms quantity in (14) did not influence neither fundamental functions nor their second derivatives. The employed dependences $q(w)$ are shown in Figure 4. They show the forms w_{yy}''', F_{yy}''' (second order derivatives) with regard to axial and diagonal lines for the values $w = 0.2$ and $w = 0.4$ in the shell center (upper and lower group of curves, respectively) for $K_x = K_y = 16$ Red (green) curves correspond to the case then the shell radiation is employed from its convexity (concavity) side. In addition, blue color corresponds to the elastic–plastic solution, whereas yellow refers to the elastic solution.

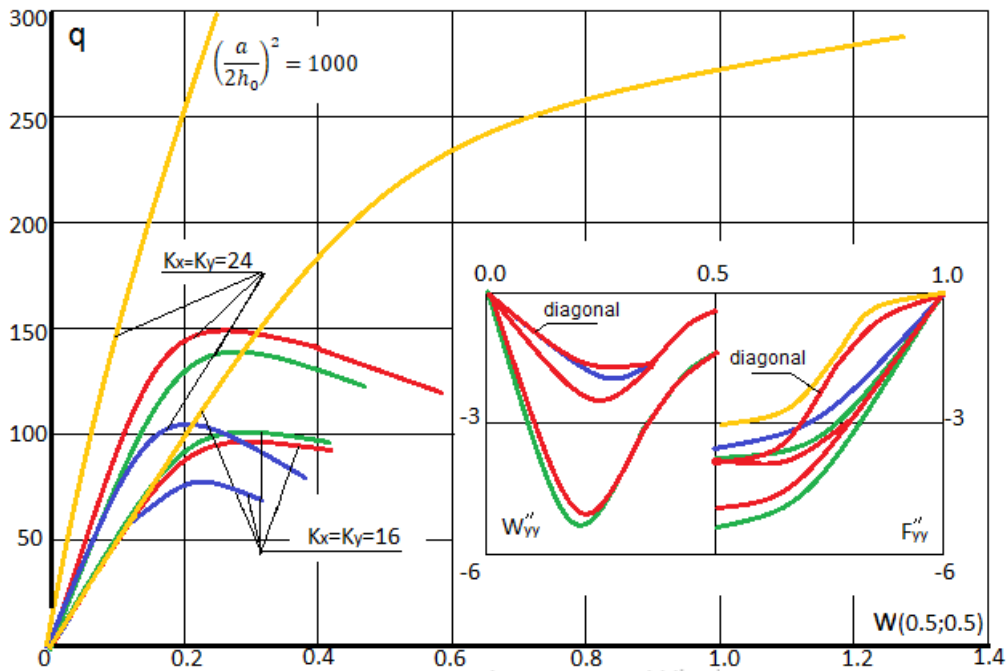


Figure 4. Load–deflection function in the shell center and shell cross-section I–I with regard to $w''_{yy} = \frac{\partial^2 w}{\partial y^2}$ and $F''_{yy} = \frac{\partial^2 F}{\partial y^2}$.

In the case of simply supported shells along their contour versus the geometric parameters K_x and K_y the radiation direction may influence the values of the upper critical loads (for instance, for $K_x = K_y = 24$ the radiation employed from the convex shell side yields increase the upper critical load in amount of 47.5%, where from its concave side it achieves 35.2% or has the negligible influence). The similar consideration hold in the case for fixed $K_x = K_y = 16$ the radiation employed from the convex shell side and from concave shell side yields increase of the upper critical load on amount of 34.6%. Distribution of the plastic zones for the plate with the fixed parameters $K_x = K_y = 16$, $K_x = K_y = 24$ along plane layers and along shell thickness for $w = 0.2$ and for $w = 0.4$ are reported in Figures 5 and 6, respectively (blue curves correspond to plastic zones for the case of the radiation lack).

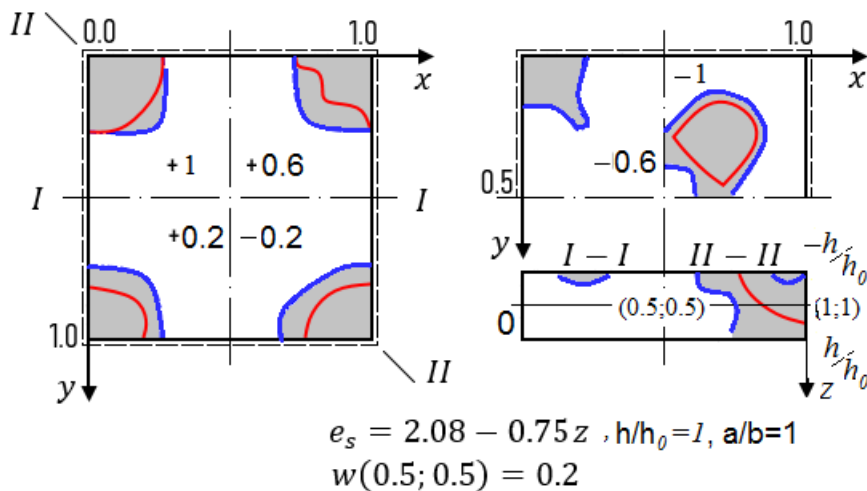


Figure 5. Views of the elastic–plastic deformation with regard to cross-section I–I and cross-section II–II along the shell thickness $h = +1; +0.6; +0.2; -0.2; -0.6; -1$ for $K_x = K_y = 16$.

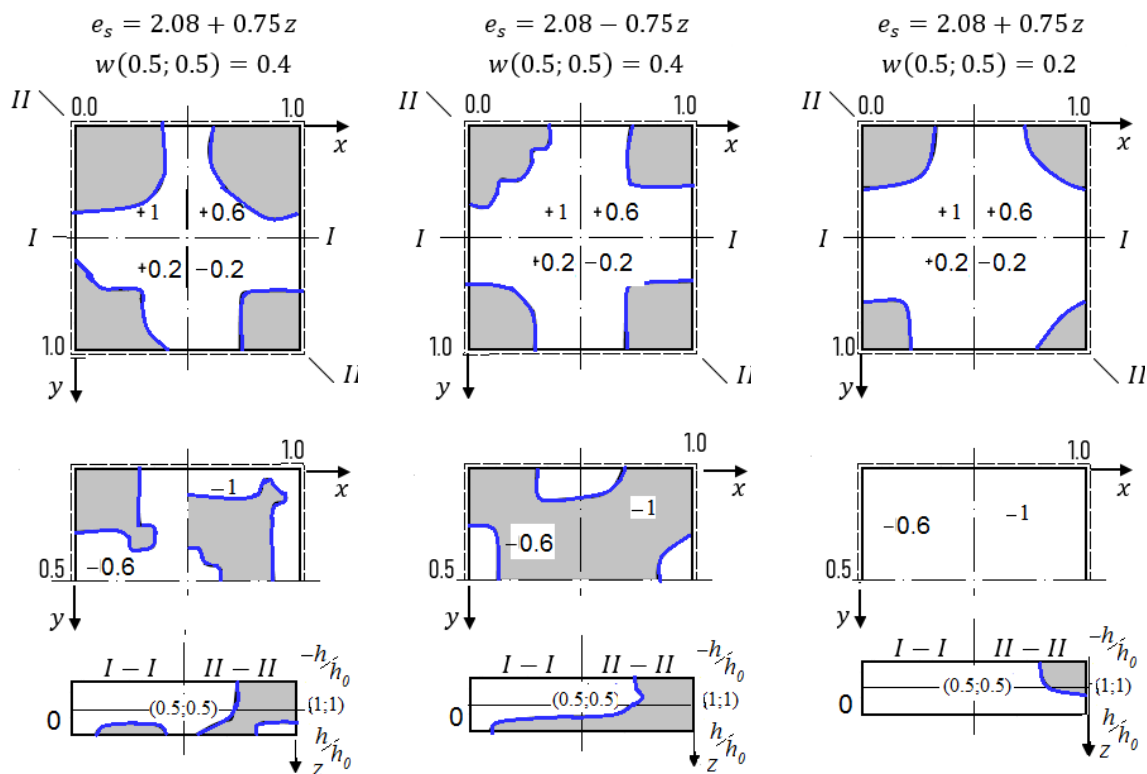


Figure 6. Views of the elastic–plastic deformation with regard to cross-section I–I and cross-section II–II along the shell thickness $h = +1; +0.6; +0.2; -0.2; -0.6; -1$ for $K_x = K_y = 24$.

7. Concluding Remarks

This work has been devoted to the mathematical modeling problem of flexible rectangular shallow shells stability under temperature field and subjected to nuclear radiations in order to improve technological and mechanical properties of the studied shells.

The developed theory and mathematical/numeric analyses allow estimating material strength and stability of structural members in two scale intervals, i.e., macro and micro scale. In the first case (macro) the engineering expected requirements refer to construction stability against the employed load as well as the mathematical exploitation longevity, whereas in the second case (micro) the critical role play sensitivity and stability of the construction working regimes under complexity of the input loading and thermal environment perturbations.

The carried out analysis based on the introduced theory and reliable computational algorithms allows formulating the following general conclusions of our research.

1. Theoretical background for analysis of the flexible nonhomogeneous shells under the radiation and temperature fields is given;
2. The method of solution to the derived nonlinear PDEs is based on the combination of the BGM in higher approximations, FDM and the Birger’s method with variable parameters;
3. We have found that radiation direction essentially influences both magnitude and the localization form of the plastic deformations—as well as the stresses magnitude in the shell middle surface;
4. The reported modeling and computational results allow to employ the radiation as a technological process improving the shell properties;
5. As a further study the following points are recommended for consideration:
 - (a) construction of the mathematical nonlinear models with regard to vibrations of flexible elastic–plastic MEMS elements in a temperature field under external radiation exposure;

- (b) chaotic vibrations and transition scenarios from periodic to chaotic dynamics in the conditions of temperature and radiation fields;
 - (c) development of mathematical models with an account of the relationship between the deformation and temperature fields subjected to radiation and temperature fields.
6. Experiments indicate that the mechanical properties of structural materials at certain dose of radiation (neutron fluence) are changed. These changes can be predicted by a proper and sophisticated mathematical modeling of structural members of constructions. Not accounting for the mentioned changes can lead either to excessive strength or to the appearance of additional radiation stresses and deformations, which can be economically inefficient and dangerous for structures.

Author Contributions: Conceptualization, A.V.K. and J.A.; methodology, A.V.K.; software, I.V.P.; validation, A.V.K., J.A. and V.A.K.; formal analysis, A.V.K.; investigation, J.A.; writing—original draft preparation, A.V.K.; writing—review and editing, J.A.; visualization, I.V.P.; supervision, V.A.K.; project administration, A.V.K.; funding acquisition, A.V.K. All authors have read and agreed to the published version of the manuscript.

Funding: This work was supported by the Grant Russian Foundation for Basic Research (RFBR) NO.20–08–00354.

Conflicts of Interest: The authors declare no conflicts of interest.

References

1. Dienes, G.J. Effects of nuclear radiations on the mechanical properties of solids. *J. Appl. Phys.* **1953**, *24*, 315–319. [[CrossRef](#)]
2. Remnev, Y.I. On stresses in metals during irradiation. *New High. Sch. Fiz. Mat.* **1958**, *4*, 91–98.
3. Remnev, Y.I. On the calculation of volumetric changes in metals upon neutron irradiation. *Her. Mosc. St. Univ.* **1959**, *1*, 12–17.
4. Lensky, V.S. The effect of reactive irradiation on the mechanical properties of solids. *Eng. Coll.* **1960**, *28*, 17–23.
5. Ilyushin, A.A.; Ogibalov, P.M. On the strength of the shells of a thick-walled cylinder and a hollow ball subjected to irradiation. *Eng. Coll.* **1960**, *28*, 134–144.
6. Norris, D.I.R. The use of the high voltage electron microscope to simulate fast neutron-induced void swelling in metals. *J. Nucl. Mater.* **1971**, *40*, 66–76. [[CrossRef](#)]
7. Likhachev, Y.I.; Pupko, V.Y. *Strength of Fuel Elements of Nuclear Reactors*; Atomizdat: Moscow, Russia, 1975. (In Russian)
8. Singh, B.N.; Horsewell, A.; Gelles, D.S.; Garner, F.A. Void swelling in copper and copper alloys irradiated with fission neutrons. *J. Nucl. Mater.* **1992**, *191–194*, 1172–1176. [[CrossRef](#)]
9. Singh, B.N.; Horsewell, A.; Toft, P. Effects of neutron irradiation on microstructure and mechanical properties of pure iron. *J. Nucl. Mater.* **1999**, *271–272*, 97–101. [[CrossRef](#)]
10. Garner, F.A.; Makenas, B.J.; Chastain, S.A. Swelling and creep observed in AISI 304 fuel pin cladding from three MOX fuel assemblies irradiated in EBR-II. *J. Nucl. Mater.* **2011**, *413*, 53–61. [[CrossRef](#)]
11. Shea, H.R. Effects of radiation on MEMS. In *Reliability, Packaging, Testing, and Characterization of MEMS/MOEMS and Nanodevices X*; SPIE: Cergy France, 2011; Volume 7928. [[CrossRef](#)]
12. Ghorbanpour Arani, A.; Ahmadi, M.; Ahmadi, A.; Rastgoo, A.; Sepyani, H.A. Buckling analysis of a cylindrical shell, under neutron radiation environment. *Nucl. Eng. Des.* **2012**, *242*, 1–6. [[CrossRef](#)]
13. Sercombe, J.; Aubrun, I.; Nonon, C. Power ramped cladding stresses and strains in 3D simulations with burnup-dependent pellet-clad friction. *Nucl. Eng. Des.* **2012**, *242*, 164–181. [[CrossRef](#)]
14. De Pauw, B.; Lamberti, A.; Ertveldt, J.; Rezayat, A.; Van Tichelen, K.; Vanlanduit, S.; Berghmans, F. Vibration monitoring using fiber optic sensors in a lead-bismuth eutectic cooled nuclear fuel assembly. *Sensors* **2016**, *16*, 571–576. [[CrossRef](#)]
15. Sitepu, E.C.; Sembiring, T.; Sebayang, K.; Sumirat, I.; Rianna, M.; Marlianto, E.; Sukaryo, S.G. A study of the use of palm fiber and palm shell as a thermal neutron radiation shielding material. *Case Stud. Therm. Eng.* **2019**, *14*, 100468. [[CrossRef](#)]

16. Greco, L.; Cuomo, M.; Contrafatto, L. Two new triangular G1-conforming finite elements with cubic edge rotation for the analysis of Kirchhoff plates. *Comput. Methods Appl. Mech. Eng.* **2019**, *356*, 354–386. [CrossRef]
17. Balobanov, V.; Kiendl, J.; Khakalo, S.; Niiranen, J. Kirchhoff–Love shells within strain gradient elasticity: Weak and strong formulations and an H3-conforming isogeometric implementation. *Comput. Methods Appl. Mech. Eng.* **2019**, *344*, 837–857. [CrossRef]
18. Srour, J.R.; Marshall, C.J.; Marshall, P.W. Review of displacement damage effects in silicon devices. *IEEE Trans. Nucl. Sci.* **2003**, *50*, 653–670. [CrossRef]
19. Babich, D.V. The Stress-Strain State of Thin-Walled Structures Exposed to Radiation. *Int. Appl. Mech.* **2003**, *39*, 953–960. [CrossRef]
20. Marchal, N.; Campos, C.; Garnier, C. Finite element simulation of Pellet-Cladding Interaction (PCI) in nuclear fuel rods. *Comput. Mater. Sci.* **2009**, *45*, 821–826. [CrossRef]
21. Semenov, A.A.; Woo, C.H. Modeling dislocation structure development and creep–swelling coupling in neutron irradiated stainless steel. *J. Nucl. Mater.* **2009**, *393*, 409–417. [CrossRef]
22. Karahan, A.; Buongiorno, J. A new code for predicting the thermo-mechanical and irradiation behavior of metallic fuels in sodium fast reactors. *J. Nucl. Mater.* **2010**, *396*, 283–293. [CrossRef]
23. Hall, M.M. Stress state dependence of in-reactor creep and swelling: Part I: Continuum plasticity model. *J. Nucl. Mater.* **2010**, *396*, 112–118. [CrossRef]
24. Williamson, R.L. Enhancing the ABAQUS thermomechanics code to simulate multipellet steady and transient LWR fuel rod behavior. *J. Nucl. Mater.* **2011**, *415*, 74–83. [CrossRef]
25. Karthik, V.; Murugan, S.; Parameswaran, P.; Venkiteswaran, C.N.; Gopal, K.A.; Muralidharan, N.G.; Saroja, S.; Kasiviswanathan, K.V. Austenitic stainless steels for fast reactors -irradiation experiments, property evaluation and microstructural studies. *Energy Proc.* **2011**, *7*, 257–263. [CrossRef]
26. Fisher, H.D.; Longo, R. Creep analysis of slightly oval cylindrical shells subjected to time-dependent loading, temperature and neutron flux. *Nucl. Eng. Des.* **1978**, *48*, 437–449. [CrossRef]
27. Collaborations to Develop Miniaturization Technologies for Space Exploration. Nano and Micro Systems. Capabilities. Microdevices Laboratory. NASA Jet Propulsion Laboratory California Institute of Technology. Available online: <http://microdevices.jpl.nasa.gov/capabilities/nano-and-micro-systems/> (accessed on 27 June 2016).
28. Sandia National Laboratories. Micro-Electro-Mechanical Systems (MEMS). Available online: <http://www.sandia.gov/mstc/mems/> (accessed on 27 June 2016).
29. Dell’Isola, F.; Seppecher, P.; Spagnuolo, M.; Barchiesi, E.; Hild, F.; Lekszycki, T.; Giorgio, I.; Placidi, L.; Andreaus, U.; Cuomo, M.; et al. Advances in pantographic structures: Design, manufacturing, models, experiments and image analyses. *Contin. Mech. Thermodyn.* **2019**, *31*, 1231–1282. [CrossRef]
30. Giorgio, I.; Rizzi, N.L.; Turco, E. Continuum modelling of pantographic sheets for out-of-plane bifurcation and vibrational analysis. *Proc. R. Soc. A Math. Phys. Eng. Sci.* **2017**, *473*, 20170636. [CrossRef]
31. Giorgio, I.; Culla ADel Vescovo, D. Multimode vibration control using several piezoelectric transducers shunted with a multiterminal network. *Arch. Appl. Mech.* **2009**, *79*, 859–879. [CrossRef]
32. Birger, I.A. Some general methods for solving problems of the theory of plasticity. *Appl. Math. Mech.* **1961**, *15*, 6–10.
33. Vlasov, V.Z. *General Theory of Shells and Its Applications in Technology*; Gostekhizdat: Moscow, Russia, 1949. (In Russian)
34. Krysko, V.A.; Awrejcewicz, J.; Komarov, S.A. Nonlinear deformations of spherical panels subjected to transversal load action. *Comput. Meth. Appl. Mech. Eng.* **2005**, *194*, 3108–3126. [CrossRef]
35. Awrejcewicz, J.; Krysko, V.A. *Elastic and Thermoelastic Problems in Nonlinear Dynamics of Structural Members*, 2nd ed.; Springer: Berlin, Germany, 2020.
36. Balashevich, Y.I.; Novozhilov, V.V. The theory of plasticity, taking into account residual microstresses. *Appl. Math. Mech.* **1958**, *22*, 1–7. (In Russian)

